Advanced Materials

Multifunctional Nanohybrid Based on Porous Silicon Nanoparticles, Gold Nanoparticles and Acetalated Dextran for Liver Regeneration and Acute Liver Failure Theranostics

--Manuscript Draft--

Manuscript Number:	adma.201703393R1
Full Title:	Multifunctional Nanohybrid Based on Porous Silicon Nanoparticles, Gold Nanoparticles and Acetalated Dextran for Liver Regeneration and Acute Liver Failure Theranostics
Article Type:	Invited Communication
Section/Category:	By Invitation Only: Materials Science in Finland
Keywords:	porous silicon; nanoparticles; nanohybrids; liver regeneration; theranostic
Corresponding Author:	Helder Santos, D.Sc. (Chem. Eng.) University of Helsinki Helsinki, Helsinki FINLAND
Additional Information:	
Question	**Response**
Please submit a plain text version of your cover letter here. **If you are submitting a revision of your manuscript, please do not overwrite your original cover letter. There is an opportunity for you to provide your responses to the reviewers later; please do not add them here**.	Dr. Lorna Stimson Advanced Materials Editor Dear Dr. Stimson, As agreed before, I would like to submit our manuscript entitled “Multifunctional Nanohybrid Based on Porous Silicon Nanoparticles, Gold Nanoparticles and Acetalated Dextran for Efficient Liver Regeneration and Acute Liver Failure Theranostics” by Zehua Liu, Yunzhan Li, Dr. Wei Li, Chen Xiao, Dr. Dongfei Liu, Chao Dong, Ming Zhang, Ermei Mäkilä, Dr. Marianna Kemell, Prof. Jarno Salonen, Prof. Jouni T. Hirvonen, Prof. Hongbo Zhang, Prof. Dawang Zhou, Prof. Xianming Deng, and Prof. Hélder A. Santos, for the Special issue ‘Materials Science in Finland’ for publication as a Communication in Advanced Materials. One of the major aims in nanomedicine is the ability to perform multiple functions using the same nanocarrier, that is, the ability to target, image, diagnose and monitor disease progress using only one single nanoparticle, which is also currently under investigation for applications in hepatopathy diagnose and therapy. Moreover, nanoparticles with specific optical or imaging properties can improve the detection of different liver diseases and play an important role in therapeutic decision-making. Acute liver failure (ALF) is a clinical syndrome as a result of the rapid loss in hepatocyte functions. Due to the limited therapeutically possibilities and the lack of diagnosis/imaging methods, ALF patients represent some of the most challenging cases in terms of the level and complexity of care required. Among all the proposed biomaterials so far, porous silicon nanoparticles (PSi NPs) have been widely investigated as advanced biomaterial as it is biodegradable and biocompatible with tunable pore sizes and has a versatile surface physicochemical properties, making PSi very flexible in loading different kind of cargos for anti-cancer, diabetes, heart infraction and immunotherapy. The unique physical and optical properties of gold nanoparticles (Au NPs) have led to various schemes for developing Au NPs as a contrast-enhancing agent for computer tomography (CT), Raman, X-ray and photoacoustic imaging applications. Several papers have demonstrated the feasibility of applying CT imaging to track monocyte recruitment to tissue plaques using Au NPs as contrasting agent, and the contrasting efficiency of Au NPs is largely related with its particle size: Too small Au NPs (150 nm), despite their satisfied MPS uptake and contrasting ability, can hardly be excreted from the body and show higher cellular toxicity. To address this obstacle, it is desirable that the initial size of Au NPs is relatively small with high biocompatibility, and further be incorporated into a larger biodegradable/biocompatible matrix to reduce renal clearance and improve macrophages uptake. Once the NPs are uptaken by the MPS, which is accumulated within the plaque sites, the matrix will collapsing to release the

	Au NPs. Upon such consideration, we hypothesize the construction of a PSi/Au nanohybrid has highly potential to be applied into liver regeneration and ALF theranostics. But in order to achieve this, we need to further establish one facile, versatile method to efficiently encapsulate both particles within one single carrier at the same time. Herein, we report a novel nanohybrid-based on PSi, Au NPs and acetalated dextran (DPSi/DAu@AcDEX) to effectively encapsulate and deliver one drug and increase the CT signal for ALF theranostics, using a microfluidic-assisted single-step co-encapsulating of different nanoparticles at the same time. By alternating the surface properties of different nanoparticles and by modulating the composition of the organic phase, we effectively encapsulated both PSi and Au NPs into the polymer matrix simultaneously, thus further achieving a multifunctional application. In summary, we have successfully prepared a PSi-based nanohybrid composite for liver regeneration and ALF treatment. This system can be used to identify pathologically changes in the tissues and selectively deliver drugs to these sites, which have an extremely high potential to ameliorate therapeutic outcomes for patients. It also effectively loads the therapeutic compound (XMU-MP-1) inside, which greatly improves the drug solubility, precise in situ drug delivery and the drug functioning time. In vivo results confirmed the superior treatment effect and better compliance of this newly developed nanoformulation than free compound. Considering our data, the application of our nanosystem appears to play a crucial role in targeting the lesion area, thus an increased local drug concentration may attribute to the improved ALF reverse effect. Moreover, the residence of Au particles within the matrix further endows our system for CT-imaging, which shows promise to diagnose ALF at an early stage. Altogether, these results support that the developed nanohybrid has a potential theranostic platform for ALF. This work brings together several scientific areas, including materials science, biomedical engineering, biomaterials, drug delivery, and bio-imaging by NPs. This new result is completely covered within the scope of Advanced Materials and is of timely interest to the readers of this journal. We firmly believe that this manuscript is suitable for publishing in Advanced Materials. We truly declare that the present article and its contents have not been previously published in any language anywhere by any of the present authors and are not also under simultaneous consideration in another journal at the time of this submission. Thank you for your consideration. Sincerely yours, Hélder Santos Associate Professor Dr. Hélder A. Santos, D.Sc. (Chem. Eng.) Head of the Pharmaceutical Nanotechnology and Chemical Microsystems Unit Head of Preclinical Drug Formulation and Analysis Group Drug Research Program, Faculty of Pharmacy, University of Helsinki, Finland & Helsinki Institute of Life Science (HiLIFE), University of Helsinki, Finland Email: helder.santos@helsinki.fi http://www.helsinki.fi/~hsantos/ https://scholar.google.com/citations?hl=en-EN&user=K3Pj_gwAAAAJ
Do you or any of your co-authors have a conflict of interest to declare?	No. The authors declare no conflict of interest.
Corresponding Author Secondary Information:	
Corresponding Author's Institution:	University of Helsinki
Corresponding Author's Secondary Institution:	

First Author:	Zehua Liu
First Author Secondary Information:	
Order of Authors:	Zehua Liu
	Yunzhan Li
	Wei Li
	Chen Xiao
	Dongfei Liu
	Chao Dong
	Ming Zhang
	Ermei Mäkilä
	Marianna Kemell
	Jarno Salonen
	Jouni Hirvonen
	Hongbo Zhang
	Dawang Zhou
	Xianming Deng
	Helder Santos, D.Sc. (Chem. Eng.)
Order of Authors Secondary Information:	
Abstract:	Herein, we report a novel nanohybrid-based on porous silicon, gold NPs and acetalated dextran(DPSi/DAu@AcDEX) to effectively encapsulate and deliver one drug and increase the CT signal for acute liver failure(ALF) theranostics. Microfluidic-assisted method is used to encapsulate NPs into a polymer matrix, using a single-step co-encapsulating of different NPs at the same time. By alternating the surface properties of different NPs and by modulating the composition of the organic phase, we effectively encapsulated both PSi and Au NPs into the polymer matrix simultaneously, thus further achieving a multifunctional application. This system can be used to identify pathologically changes in the tissues and selectively deliver drugs to these sites. It also effectively loads the therapeutic compound(XMU-MP-1) inside, improving the drug solubility, precise in situ drug delivery and the drug functioning time. In vivo results confirmed the superior treatment effect and better compliance of this newly developed nanoformulation than free compound. This nanosystem plays a crucial role in targeting the lesion area, thus increasing the local drug concentration important for ALF reverse effect. Moreover, the residence of Au NPs within the matrix further endows our system for CT-imaging. Altogether, these results support that this nanohybrid has a potential theranostic platform for ALF.

WILEY-VCH

DOI: 10.1002/ ((please add manuscript number))

Multifunctional Nanohybrid Based on Porous Silicon Nanoparticles, Gold Nanoparticles and Acetalated Dextran for Liver Regeneration and Acute Liver Failure Theranostics

Zehua Liu [†], Yunzhan Li [†], Wei Li [†], Chen Xiao, Dongfei Liu, Chao Dong, Ming Zhang, Ermei Mäkilä, Marianna Kemell, Jarno Salonen, Jouni T. Hirvonen, Hongbo Zhang, Dawang Zhou*, Xianming Deng * and Hélder A. Santos **

[*] Z. Liu, Dr. W. Li, Dr. D. F. Liu, Prof. J. T. Hirvonen and Prof. H. A. Santos
Division of Pharmaceutical Chemistry and Technology, Drug Research Program
Faculty of Pharmacy, University of Helsinki
FI-00014, Helsinki, Finland
E-mail: helder.santos@helsinki.fi (H. A. Santos)

[*] Prof. H. A. Santos
Helsinki Institute of Life Science (HiLIFE)
University of Helsinki
FI-00014, Helsinki, Finland

[*] Y. Z. Li, C. Xiao, M. Zhang, C. Dong, Prof. D. Zhou and Prof. X. Deng
State Key Laboratory of Cellular Stress Biology, Innovation Center for Cell Signaling Network, School of Life Sciences, Xiamen University
361101, Fujian, China
E-mail: xmdeng@xmu.edu.cn (X. Deng), dwzhou@xmu.edu.cn (D. Zhou)

[*] Y. Z. Li, C. Xiao, M. Zhang, C. Dong, Prof. D. Zhou and Prof. X. Deng
State-Province Joint Engineering Laboratory of Targeted Drugs from Natural Products, School of Life Sciences, Xiamen University
361101, Fujian, China

[*] Prof. H. Zhang
Department of Pharmaceutical Science, Åbo Akademi University
FI-20520, Turku, Finland
E-mail: hongbo.zhang@abo.fi (H. Zhang)

[*] Prof. H. Zhang
Turku Center of Biotechnology, Åbo Akademi University
FI-20520, Turku, Finland

Dr. D. Liu
School of Applied Science and Engineering
Harvard University
MA 02138, Cambridge, USA

E. Mäkilä, Prof. J. Salonen
Laboratory of Industrial Physics, Department of Physics, University of Turku
FI-20014, Turku, Finland

Dr. M. Kemell
Department of Chemistry, University of Helsinki
FI-00014, Helsinki, Finland

Keywords: porous silicon; nanoparticles; nanohybrids; liver regeneration; theranostic

One of the major aims in nanomedicine is the ability to perform multiple functions using the same nanocarrier, that is, the ability to target, image, diagnose and monitor disease progress using only one single nanoparticle, which is also currently under investigation for applications in hepatopathy diagnose and therapy.[1, 2] A large variety of drugs can be associated to nanocarriers to enable liver-targeted drug delivery. Compared with other methods, the treatment plan involving the use of multifunctional nanoparticles holds the promise of more accurately targeted treatment, with a higher likelihood of a successful outcome.[3-5] Moreover, nanoparticles with specific optical or imaging properties, such as gold nanoparticles[3], iron oxides[6], and alkaline earth metal-based nanoparticles[7] can improve the detection of different liver diseases and play an important role in therapeutic decision-making.

Acute liver failure (ALF) is a clinical syndrome as a result of the rapid loss in hepatocyte functions. Due to the limited therapeutically possibilities and the lack of diagnosis/imaging methods, ALF patients represent some of the most challenging cases in terms of the level and complexity of care required.[8] Despite the recently promising results brought by the newly developed small molecules, the lack of a proper drug delivery method may greatly impact their further application and the inherent limitation of conventional imaging methods for ALF makes the treatment process monitoring very difficult.[9] Therefore, a novel nanohybrid-based theranostic platform is urgently needed to solve the aforementioned problems.

Among all the proposed biomaterials so far, porous silicon nanoparticles (PSi NPs) have been widely investigated as advanced biomaterial as it is biodegradable and biocompatible with tunable pore sizes and has a versatile surface physicochemical properties, making PSi very flexible in loading different kind of cargos for anti-cancer, diabetes, heart infraction and immunotherapy.[10-15] Moreover, within the hepatopathy care, PSi is unique from other biomaterials as recent reports showed the administration of extra silicon, which is the main composition of PSi, can effectively protect the liver from oxidative damage,[16, 17] thus making

the PSi drug delivery system very attractive for hepatopathy drug delivery, yet only very few attempts have been made to apply PSi into hepatic diseases and liver regeneration.[18]

Former clinical studies suggested abdominal computer tomography (CT) scanning can play a useful role in the management of patients with ALF,[19] and the unique physical and optical properties of gold nanoparticles (Au NPs) have led to various schemes for developing Au NPs as a contrast-enhancing agent for CT, Raman, X-ray and photoacoustic imaging applications.[20] The high atomic number and electron density of Au makes it a good candidate for CT imaging,[21] hence applying Au NPs based nanohybrids is highly potent for hepatic disease theranostics. Several papers have demonstrated the feasibility of applying CT imaging to track monocyte recruitment to tissue plaques using Au NPs as contrasting agent,[22, 23] and the contrasting efficiency of Au NPs is largely related with its particle size: Too small Au NPs (< 5nm) suffer from rapid clearance by renal filtration, leading to low plaque accumulation, and they also tend to show limited monocyte phagocytic system (MPS) uptake, resulting in an unsatisfied lesion tracking ability; whereas larger Au NPs (> 150 nm), despite their satisfied MPS uptake and contrasting ability, can hardly be excreted from the body and show higher cellular toxicity.[24] To address this obstacle, it is desirable that the initial size of Au NPs is relatively small with high biocompatibility, and further be incorporated into a larger biodegradable/biocompatible matrix to reduce renal clearance and improve macrophages uptake. Once the NPs are taken up by the MPS, which are accumulated within the plaque sites, the polymer matrix will collapse to release the Au NPs.[25, 26]

Upon such consideration, we hypothesize the construction of a PSi/Au nanohybrid has highly potential to be applied into liver regeneration and ALF theranostics. But in order to achieve this, we need to further establish one facile, versatile method to efficiently encapsulate both particles within one single carrier at the same time. Herein, we report a novel nanohybrid-based on PSi, Au NPs and acetalated dextran (DPSi/DAu@AcDEX) to effectively encapsulate and deliver one drug and increase the CT signal for ALF theranostics. Former

studies used microfluidic-assisted methods to encapsulate nanoparticles into a polymer matrix, yet there are few papers demonstrating a single-step co-encapsulating of different nanoparticles at the same time.[27, 28] In this study, by alternating the surface properties of different nanoparticles and by modulating the composition of the organic phase, we effectively encapsulate both PSi and Au NPs into the polymer matrix simultaneously, thus further achieving a multifunctional application.

Facilitated by the application of PSi, XMU-MP-1, a recently developed small molecule with the promising potential for ALF treatment (**Figure S1A**),[9] is effectively loaded inside the nanohybrid. To solve the major obstacle that ALF lacks of bio-imaging based diagnose tool, dextranylated gold nanoparticles (DAu NPs) are constructed and simultaneously entrapped into the polymer matrix alone with dextranylated PSi (DPSi). By constructing this DPSi/DAu@AcDEX nanostructure, our nanohybrids also have the ability to act as a contrasting agent for CT-imaging. Acetalated dextran (AcDEX), a biologically safe and pH-sensitive polymer, is used to form the outer polymer matrix. AcDEX is widely applied in tissue engineering, controlled drug delivery and immunomodulation for multiple reasons.[29] The introduction of outer AcDEX matrix can block the pores of PSi for the drug release, but the decomposition of AcDEX under acidic environment allows the intracellular drug release and the dormant Au NPs release, thus the size dilemma of Au NPs within plaque detection is also solved by this hierarchical strategy. Most importantly, this facile method to encapsulate different particles within one polymer matrix offers the possibilities to construct different kind of multifunctional nanohybrids. As far as we know, this is the first time investigating PSi as drug delivery system for liver regeneration and further evaluating its potent application in ALF therapy.

The approach for the construction of DPSi/DAu@AcDEX is illustrated in **Figure 1A**. We used a well-established method to synthesize AcDEX and its derivate spermine AcDEX,[30, 31] and their successful formation was confirmed by ^{1}H nuclear magnetic resonance (see

Supporting Information) spectrum. Undecylenic acid-modified thermally hydrocarbonized PSi was applied because the hydrophobic surface favors the loading of XMU-MP-1. The PSi particles were modified by spermine AcDEX to form DPSi (**Figure 1B(a)**); the introduction of spermine AcDEX can both increase its dispersity and biocompatibility and also facilitate the nucleation process to further construct the nanohybrid. Similarly, Au NPs were modified with spermine AcDEX to form DAu (**Figure 1B(b)**). The successful modification of DPSi and DAu was confirmed by Fourier transform infrared spectroscopy (FTIR) and NMR (**Figure 1C, Figure S2**). Microfluidics assisted nanoprecipitation method was carried out to construct DPSi/DAu@AcDEX, and the nanoprecipitation process was triggered by passive microfluidic mixing in a co-flow capillary microtube. The outer AcDEX layer within the microtube was formed through nucleation and nano-precipitation driven by diffusion and mixing between the solvent (ethanol/acetonitrile = 9:1, v/v) and anti-solvent (1% Poloxamer 188 water solution) streams across the interface. We previously found out that size has an important role in AcDEX encapsulation.[27] To encapsulate DPSi with a size around 200 nm, we optimized the size of bare AcDEX particles and 300 nm spherical AcDEX particles were applied in the following (**Figure 1B(c)**) encapsulation process of DPSi. Transmission electron microscopy (TEM) images indicated the successful encapsulation of PSi nanoparticles in the AcDEX matrix. As it can be seen in **Figure 1B(d)**, after encapsulation, the irregular shape and the porous structure of DPSi were fully covered and new nanohybrids with spherical morphology were formed. Energy dispersive X-ray microscopy (EDX) was carried out to further confirm the DPSi inside the AcDEX particle, where the clear peak of Si indicated the presence of DPSi. After the encapsulation, size changes from 207±10 (DPSi) to 332±3 nm (polydispersity index (PdI): 0.19±0.01 *vs.* 0.11±0.02) were detected and also the zeta (ζ)-potential values were shifted from +6.2 ± 1.0 to –31.4 ± 4.0 mV due to the fact that the amine groups on DPSi were covered by AcDEX. We further encapsulated DAu together with DPSi. The surface modification of Au NPs is crucial for the simultaneous encapsulation as un-

modified Au NPs (dodecane conjugated) tend not to accumulate in the polymer matrix but to disperse within the medium (**Figure S3A**). After adding DAu inside the nanohybrids, both the sphericalness and the morphology of the nanohybrids showed no significant differences. EDX spectrum confirmed the co-existence of both DPSi and DAu inside AcDEX matrix, as clear Au and Si signals could be observed simultaneously in the same particle (**Figure 1B(e,f)**). The size of the final DPSi/DAu@AcDEX composite was increased to 473 ± 13 nm comparing to 332 nm for DPSi@AcDEX, whereas the ζ-potential values did not have clear changes (–33.2 ± 0.7 mV), which partially suggests that the DAu (+ 11.5 ± 1.9 mV) was more likely to be encapsulated inside the polymer matrix (**Figure 1C**). FTIR results also partially confirmed the successful encapsulation of DPSi as well as DAu (**Figure 1D**). After the modification of PSi, the DPSi spectrum showed a decrease in the band at 1720 cm^{-1}, which is the typical band for carboxyl, and a new band at 1530 cm^{-1} was observed due to the formation of amide bonds. After the AcDEX encapsulation the typical band from DPSi disappeared and was replaced by the bands from AcDEX. This is different from simple physical mixture, wherein the typical carboxyl band from DPSi (1720 cm^{-1}) is still visible (**Figure S3**). To evaluate whether the surface modification and drug loading affected the encapsulation process, we used different surface functionalized DPSi to construct the same structure, and the results showed that neither the conjugation of the fluorescence dye (Alexa Fluor® 488, **Figure S4B**), conjugation of peptide (R8 cell penetration peptide, **Figure S4C**), nor the loading of the drug (**Figure S4D,E**) affected the formation of the nanohybrids. Most importantly, even at the different PSi/Au ratios, similar nanostructures could be constructed (DPSi/DAu = 1:5, w/w, **Figure 1B(f)**, DPSi/DAu = 1:1, w/w, **Figure S4F**) without obvious free Au NPs within the medium. All this suggested robust reproducibility of the method for nanohybrids construction.

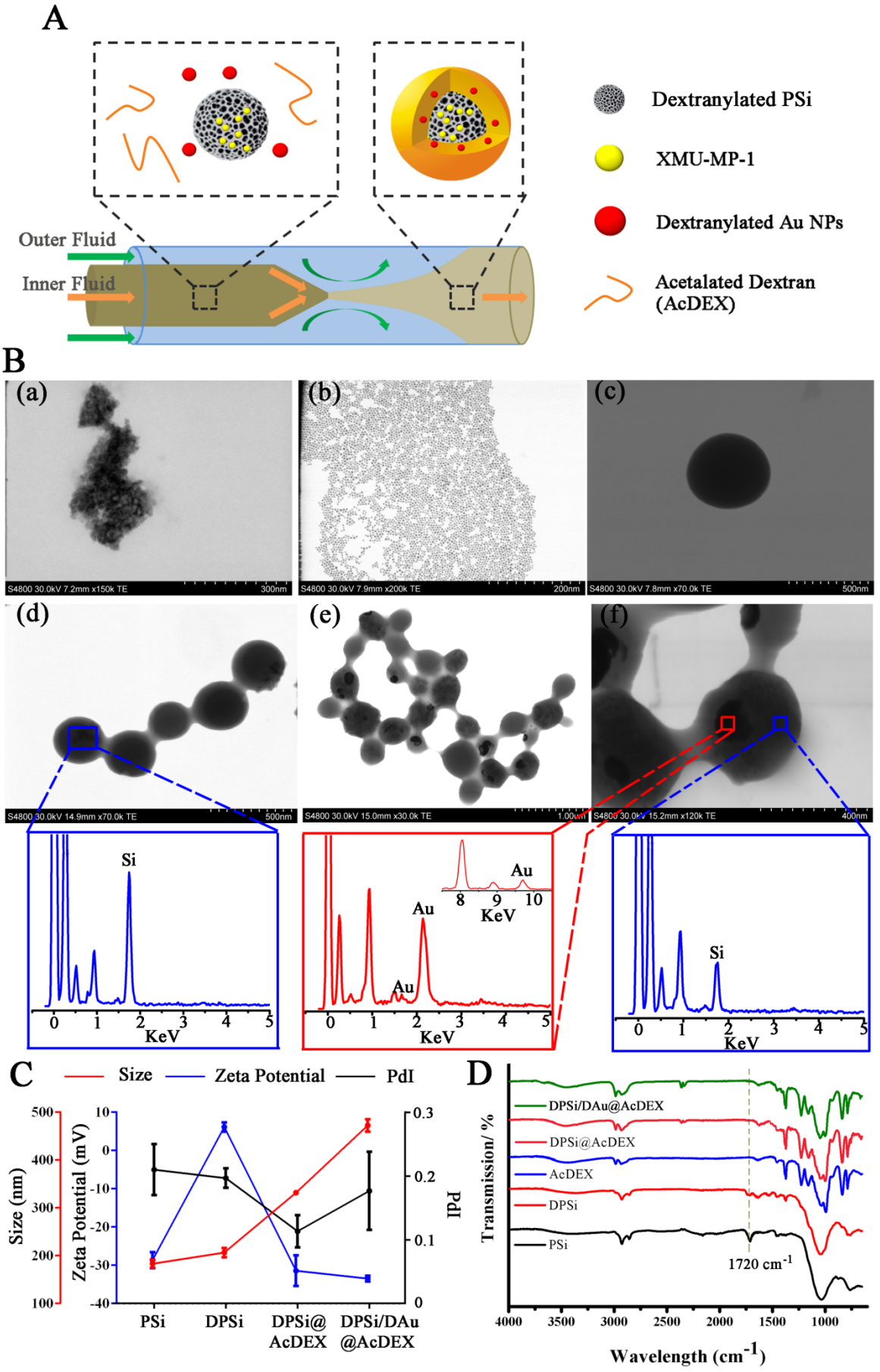
A
Outer Fluid
Inner Fluid
Dextranylated PSi
XMU-MP-1
Dextranylated Au NPs
Acetalated Dextran (AcDEX)
B
(a)
(b)
(c)
(d)
(e)
(f)
Si
Au
KeV
C
Size
Zeta Potential
PdI
Size (nm)
Zeta Potential (mV)
IPd
PSi
DPSi
DPSi@ AcDEX
DPSi/DAu @AcDEX
D
DPSi/DAu@AcDEX
DPSi@AcDEX
AcDEX
DPSi
PSi
1720 cm-1
Transmission/ %
Wavelength (cm-1)

Figure 1. Preparation and Characterization of DPSi/DAu@AcDEX. (A) Schematic illustration of the procedure to prepare the DPSi/DAu@AcDEX by microfluidics. **(B)** TEM images showing morphologies of (a) DPSi, (b) DAu, (c) AcDEX template particle, (d) DPSi@AcDEX, (e,f) DPSi/DAu@AcDEX at each step and the corresponding EDX spectrum. **(C)** Size (nm), PdI and surface zeta potentials (mV) values at each synthesis step. **(D)** FTIR spectra of PSi, DPSi, AcDEX, DPSi@AcDEX and DPSi/DAu@AcDEX, suggesting the encapsulation process.

We further investigated the drug loading and releasing profile of XMU-MP-1 loaded DPSi/DAu@AcDEX (MP@DPSi/DAu@AcDEX) *in vitro*. XMU-MP-1 is a highly insoluble drug in different solvents and it is very difficult to be administered (**Table S1**). PSi has been showed to have the ability to improve the *in vivo* drug bioavailability, especially for hydrophobic drug.[32] Without the application of DPSi, by using the same drug encapsulation procedure, the drug loading degree within the AcDEX matrix is as low as 0.04%. With DPSi, we achieved a final loading degree of 7.8% for XMU-MP-1 within the nanohybrid. Due to the coverage of AcDEX layer, the drug loaded inside the DPSi is hardly released at the physiological conditions, thus preventing the premature drug release. However, AcDEX slowly degrades at pH 7.4, thus we can detect insignificant XMU-MP-1 release after 24 h (**Figure S5A**). At pH 5.0, the AcDEX shell rapidly dissolved through decomposition of the acetal bonds and regenerating of the water-soluble dextran; and therefore, the pores were exposed to the outer solution and the drug was released (**Figure 2A**). Liver is a highly promising organ for nanocarrier-based targeting as it is the major accumulation place for nanoparticles.[33-35] Within the liver microarchitecture, blood flow is significantly slower than in the systemic circulation. The reduced velocity promotes preferential nanomaterial accumulation within the liver sinusoid, and the prevailing assumption suggests that the

majority of the particles are taken up by the stationary Kupffer cells or internalized by the patrolling macrophages and further transfer to liver.[34-36] To better simulate this condition, we conducted cellular level drug release studies by co-incubating the particles and macrophages (KG1). **Figure 2B** shows that within the blank medium, few drug can be detected to be released from the particles, but when the KG1 cells were added, the drug released to the medium had a significant augment after 3 h. The rationale behind this is when the particle is internalized by the macrophages, the AcDEX matrix will degrade within endosomes and further release the drug, small molecule XMU-MP-1 with high permeability could penetrate through the membrane of KG1 and potentially reach to hepatocytes.

We further investigated the potential of liver regeneration effect of our system *in vitro*. XMU-MP-1 effectively inhibits the Sterile 20–like kinases MST1 and MST2 (MST1/2) activities in a variety of cells.[9] MST1/2 inhibition leads to the dephosphorylation of MOB, the specific substrate of MST1/2, and further suppresses Yes-associated protein (YAP) phosphorylation, thereby activating the downstream effector YAP and promoting cell growth.[37, 38] **Figure 2C** demonstrates that our nanoformulation of XMU-MP-1 can potently inhibit MOB, and YAP phosphorylation in H_2O_2 treated cells. Comparing to free drug, our system presents a sustained functional behavior after 6 h. The proliferation effect was further tested on hepatocytes/macrophages co-culture model. Different hepatocytes/macrophages ratios were tested, and the hepatocytes/macrophages = 2/1 system was further used in the following experiments according to previous reports (**Figure S5B**).[39]

Two different administration methods were investigated separately to simulate different conditions. Due to favorable flow dynamics in liver, it has been demonstrated that the nanoparticles may accumulate within the liver architecture, then the cellular-bonded particles can remain on the cellular surface, or return to the circulation or be internalized through endocytosis or phagocytosis.[35] To simulate these conditions, we directly added XMU-MP-1 with different formulations to the hepatocytes/macrophages co-culture model followed by 24

h further incubation and test the viability of hepatocytes afterwards (co-culture model). The results showed a similar proliferation augment from the drug treatment (149 ± 9.9% and 143 ± 15.1%, free drug *v.s.* MP@DPSi/DAu@AcDEX at the highest concentration). To model the situation that DPSi/DAu@AcDEX will be recognized and be taken-up by the mononuclear phagocyte system (MPS) and further transported to the liver,[34] we first co-cultured different nanohybrid formulations with the macrophages for 4 h, then the pre-treated macrophages were collected and further co-incubated with hepatocytes for another 24 h (sequence-culture model). Comparing to free drug, significant high cell viability increase was observed for MP@DPSi/DAu@AcDEX at different concentrations ($P < 0.05$) (**Figure 2D**). Importantly, the viability augment of two different cell models treated with MP@DPSi/DAu@AcDEX had a similar trend, whereas for the free drug treated group, the sequence-culture model barely showed a proliferation effect. This confirms the effective cell proliferation augment of our nanohybrids at different conditions.

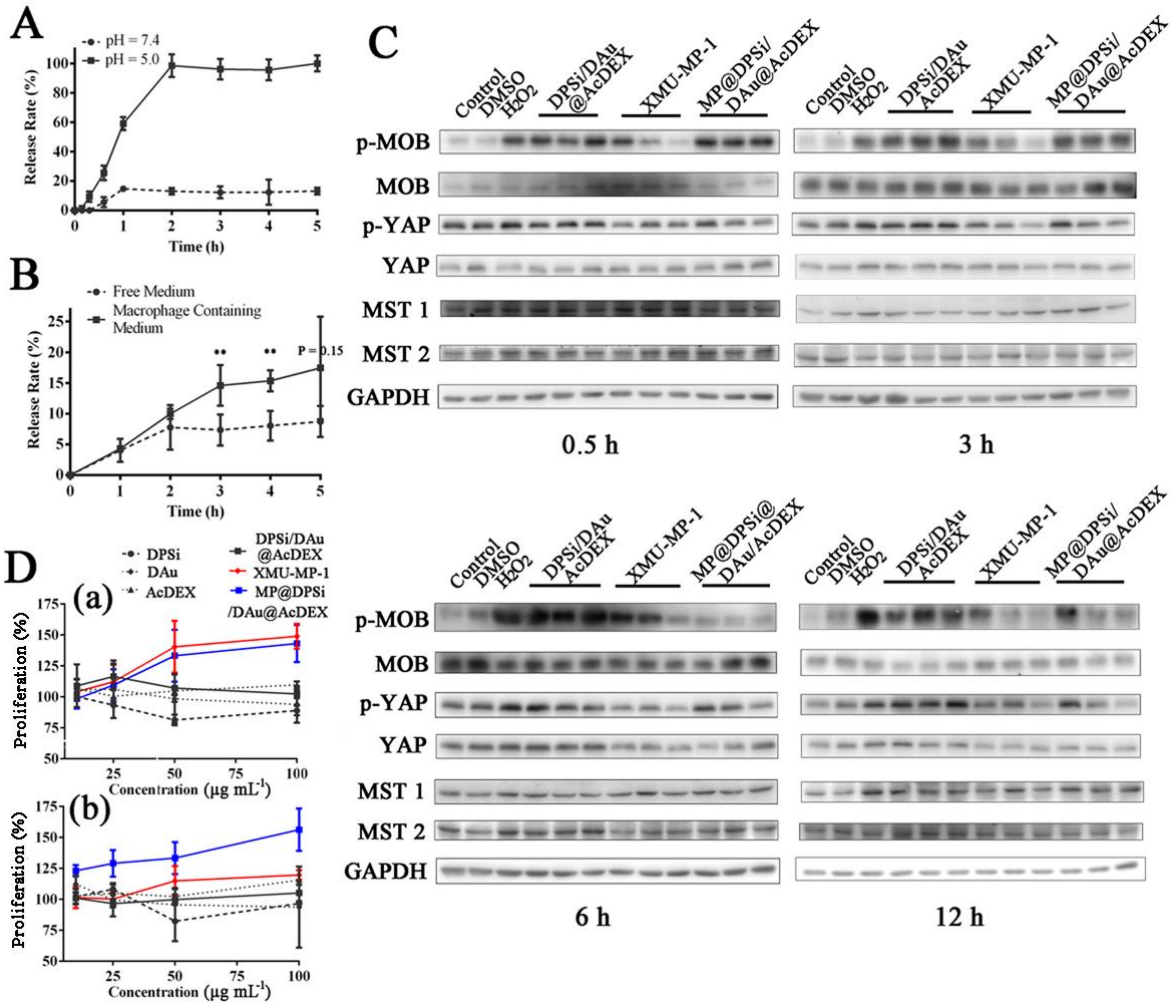

Figure 2. (A) *In vitro* XMU-MP-1 release curves at pH 5 and pH 7.4 in phosphate buffer saline (PBS) containing 5% P-188 at 37 °C within 5 h. **(B)** The XMU-MP-1 release curve at Roswell Park Memorial Institute (RPMI) medium containing KG1 macrophages at 37 °C within 5 h. **(C)** Relative phosphorylation levels of MOB and YAP (p-MOB and p-YAP) in HepG2 were probed at various concentrations of XMU-MP-1 with different formulation treatments over time (1.5 to 12 h). The corresponding pannels (from left to right) are: control, dimethyl sulfoxide (DMSO)–treated control, H_2O_2-treated control, DPSi/DAu@AcDEX with low, medium and high concentration (from left to right), free XMU-MP-1 (1, 3, and 10 μM from left to right, dissolved in DMSO), and MP@DPSi/DAu@AcDEX (containing the same amount of XMU-MP-1 at the corresponding concentration). **(D)** Cell viability of HepG2 cells **(a)** directly incubate different formulations of XMU-MP-1 with HepG2/KG1 co-culture

model for 24 h and **(b)** incubation of different formulations of XMU-MP-1 with KG1 for 4 h followed by harvesting the pre-treated KG1 cells and continuing the HepG2/KG1 co-culture model for 24 h. All the data sets were compared with the respective control. The concentration indicates the amount of DPSi/DAu@AcDEX. Data are shown as mean ± SD ($n \geq 3$), $^{*}P < 0.05$ and $^{**}P < 0.01$.

Following the promising results *in vitro*, we moved to *in vivo* studies. Phosphorylation levels of key proteins MOB and YAP (p-MOB and p-YAP) in lysates of livers from wild-type mice treated with different formulations of XMU-MP-1 over time were firstly evaluated. **Figure 3A** shows the effective suppression of p-MOB and p-YAP, and importantly our nanoformulation of XMU-MP-1 exhibited longer effecting time comparing with the free drug. We further tested the effect of our system on ALF mouse model. ALF model was established by the overdosed administration of acetaminophen (APAP), which is also a common cause of ALF worldwide.[40] After 2.5 h of the APAP gavage, XMU-MP-1 was administrated intravenously (*i.v.*) in different nanoformulations at different concentrations twice daily (**Figure 3B**). Serum alanine aminotransferase (ALT) and aspartate transaminase (AST) levels were measured at different time points to study the hepatic function with robust reliability (**Figure S6**). After 12 h, the ALT levels with values of 2056 ± 326.7 *vs.* 36 ± 4.9 and the AST levels with values of 704 ± 124.6 *vs.* 36 ± 6.1 exhibited a boost increase comparing to healthy mice and macroscopic lesion parts were observed after 24 h (**Figure S7**), suggesting the successful establishment of the ALF model. After 12 h, XMU-MP-1 treatment can alleviate the damage in a dose-dependent manner. However, free drug at both doses of 0.1 mg kg^{-1} and 0.5 mg kg^{-1} did not present a significant difference with ALF control group, whereas for the MP@DPSi/DAu@AcDEX, both concentrations showed a significant decrease of ALT and AST levels (except for AST value at low concentration, **Figure 3C(a)**). When the treatment

time extended to 24 h, ALT/AST levels in mice treated with MP@DPSi/DAu@AcDEX was markedly lower than free drug at both low dosage (890 ± 208.9 *vs.* 99 ± 29.9 for ALT, $P < 0.01$ and 318 ± 82.7 *vs.* 103 ± 16.8 for AST, $P < 0.05$) and high dosage (328 ± 79.0 *vs.* 52 ± 27.7 for ALT, $P < 0.05$ and 298 ± 66.7 *vs.* 127 ± 19.0 for AST, $P < 0.05$), indicating the superior improvement of therapeutic efficacy over free drug (**Figure 3C(b)**). Hematoxylin-eosin (H&E) staining (**Figure S8**) and TdT-mediated dUTP Nick-End labeling (TUNEL) staining (**Figure 3D**) at the corresponding time points qualitatively indicated the ALF reverse and protection of liver damage by MP@DPSi/DAu@AcDEX to a remarkable extent in terms of lesion area, whereas free drug exhibited limited function. Furthermore, immunoblots results also suggest a better treatment effect from drug-loaded DPSi/DAu@AcDEX (**Figure 3E**). At the time point of 72 h, despite the serological index showed similar liver recovery, from the TUNEL staining, mice treated with MP@DPSi/DAu@AcDEX had less scar structure, indicating a better rehabilitation (**Figure 3C(c)** and **3D**). Moreover, at the drug dose of 3 mg kg^{-1} via *i.v.*, mice mortality appeared when treated with free drug, which may be caused by the heart failure as a result of thrombus by drug precipitation. To confirm this, C-X-C chemokine receptor type 4 (CXCR-4) immunohistochemical staining (**Figure 3F**) and TUNEL staining (**Figure S9**) heart sections at 72 h after administrating free drug or MP@DPSi/DAu@AcDEX were checked to reveal the potential cardiac damage. Comparing to the free drug group, no obvious myocardial infarction was observed after injecting MP@DPSi/DAu@AcDEX at the same dosage, which further demonstrates the enhanced compliance of our nanohybrid formulation.

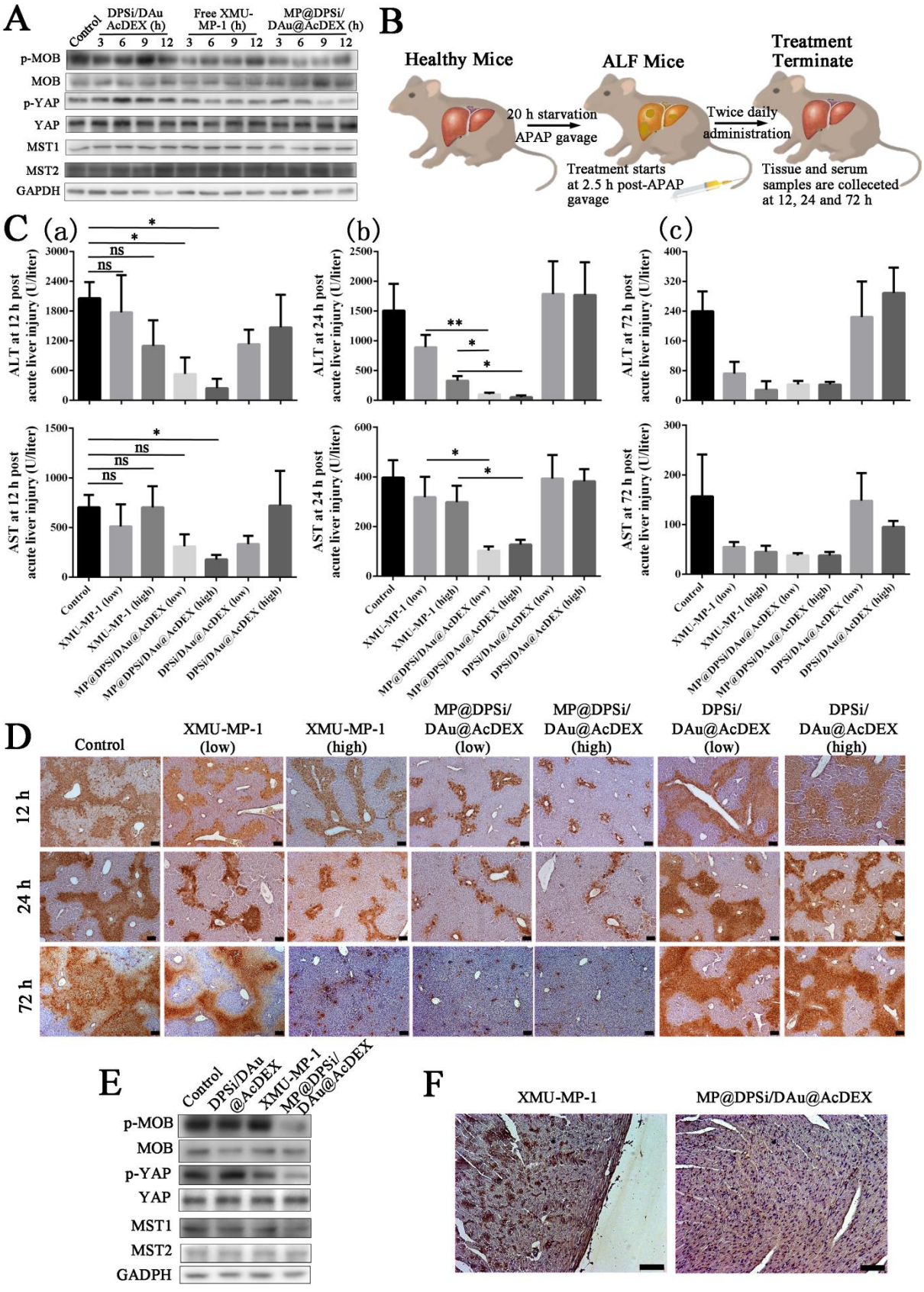

Figure 3. (**A**) Immunoblots of p-MOB and p-YAP in lysates of livers from wild-type mice treated with XMU-MP-1 (0.1 mg kg^{-1}) with different formulations over time (3 to 12 h). **(B)**

Schematics of drug evaluation in ALF model. **(C)** Serum ALT and AST levels at 12, 24, and 72 h after APAP administration among wild-type mice, followed by intravenously injection of 15% Solutol® HS 15 (control), free XMU-MP-1 (0.1 mg kg^{-1} as low concentration, 0.5 mg kg^{-1} as high concentration, and free XMU-MP-1 is prepared by dissolving the drug into 15% Solutol® HS 15 at corresponding concentration), MP@DPSi/DAu@AcDEX (containing the same amount of XMU-MP-1 at low and high concentrations respectively), and blank DPSi/DAu@AcDEX at corresponding concentration. ALF model is established by 200 mg kg^{-1} APAP gavage administration. The treatment was initiated 2.5 h post APAP gavage. Drug is administrated twice daily for 3 days. Data are shown as mean ± SEM (n = 4); $^{*}P < 0.05$ and $^{**}P < 0.01$ (Student's t-test). **(D)** TUNEL staining of liver sections at different time-points. ALF establish method and drug administration method are described above. All scale bars indicates 100 μm. **(E)** Immunoblots of p-MOB and p-YAP in lysates of livers from ALF mice treated with XMU-MP-1 (0.1 mg kg^{-1}) with different formulations at 24 h post-ALF establishment. **(F)** CXCR-4 immunohistochemical staining heart sections at 72 h after administrating free drug or MP@DPSi/DAu@AcDEX (with 3 mg kg^{-1} of XMU-MP-1), suggesting the potential cardiac damage from the free drug administration. All scale bars indicate 100 μm.

The potential rationale for the enhanced treatment index of MP@DPSi/DAu@AcDEX may be due to the lesion site specific accumulation of DPSi/DAu@AcDEX. It is well documented that following the occurrence of ALF, innate immune cells are recruited in a short time to the damage part to clear necrotic tissue and initiate the wound healing process.[41, 42] Immunofluorescence imaging demonstrates that for healthy mice macrophages were evenly distributed all over the liver, whereas for ALF mice the macrophages vastly concentrated at the specific area. Using fluorescence labeled DPSi/DAu@AcDEX, we observed the co-

localization of our particles within the macrophages, and due to that our nanohybrids also accumulate within this specific region (**Figure 4A**). **Figure 4B** further confirmed the post-ALF model establishment, a clear tendency of macrophages infiltration and enrichment was observed within necrotic plaque. So it is reasonable to assume the enhanced drug concentration within the damage area is induced by the increased local particles accumulation. In addition to that, due to the incorporated DAu within DPSi/DAu@AcDEX, we may apply the "Trojan horse" strategy into lesion detection and characterization. Early ALF lacks of proper bioimaging guided diagnostic method due to the initial damage may not induce detectable morphology changes in liver, thus introducing a proper contrasting agent is rather crucial.[43-45] Au NPs induce a strong X-ray attenuation and obsess unique physical, chemical, and biological properties, which make them an ideal candidate as CT-contrasting agents. *In vitro* CT images of aqueous dispersion of DPSi/DAu@AcDEX showed a DAu concentration dependent CT signal enhancement (**Figure 4C**). Due to the vast accumulation of macrophages within the lesion area and the major uptake of DPSi/DAu@AcDEX by macrophages, we expected to observe the lesion indication by CT-imaging. **Figure 4D(a)** showed no optical difference within ALF mice without the administration of DPSi/DAu@AcDEX, suggesting the limitation of conventional CT-imaging within ALF diagnosis. After *i.v.* injection of DPSi/DAu@AcDEX, for healthy mice, no clear signal was observed at a settled CT signal window (**Figure 4D(b)**). When defined the signal window to a relatively lower range, we observed that DAu are evenly distributed all over the liver (**Figure S10**). However, for ALF mice, a distinguishable area was generated by the accumulation of DPSi/DAu@AcDEX 30 min post-injection. The rationale for the contrasting effect could be explained as after *i.v.* injecting the same amount of DPSi/DAu@AcDEX, normal liver has a decreased overall signal due to homogenous distribution of the particles as observed above, whereas damage will cause local accumulation of macrophages, which will enlarge the local signal as the residence of DPSi/DAu@AcDEX inside.

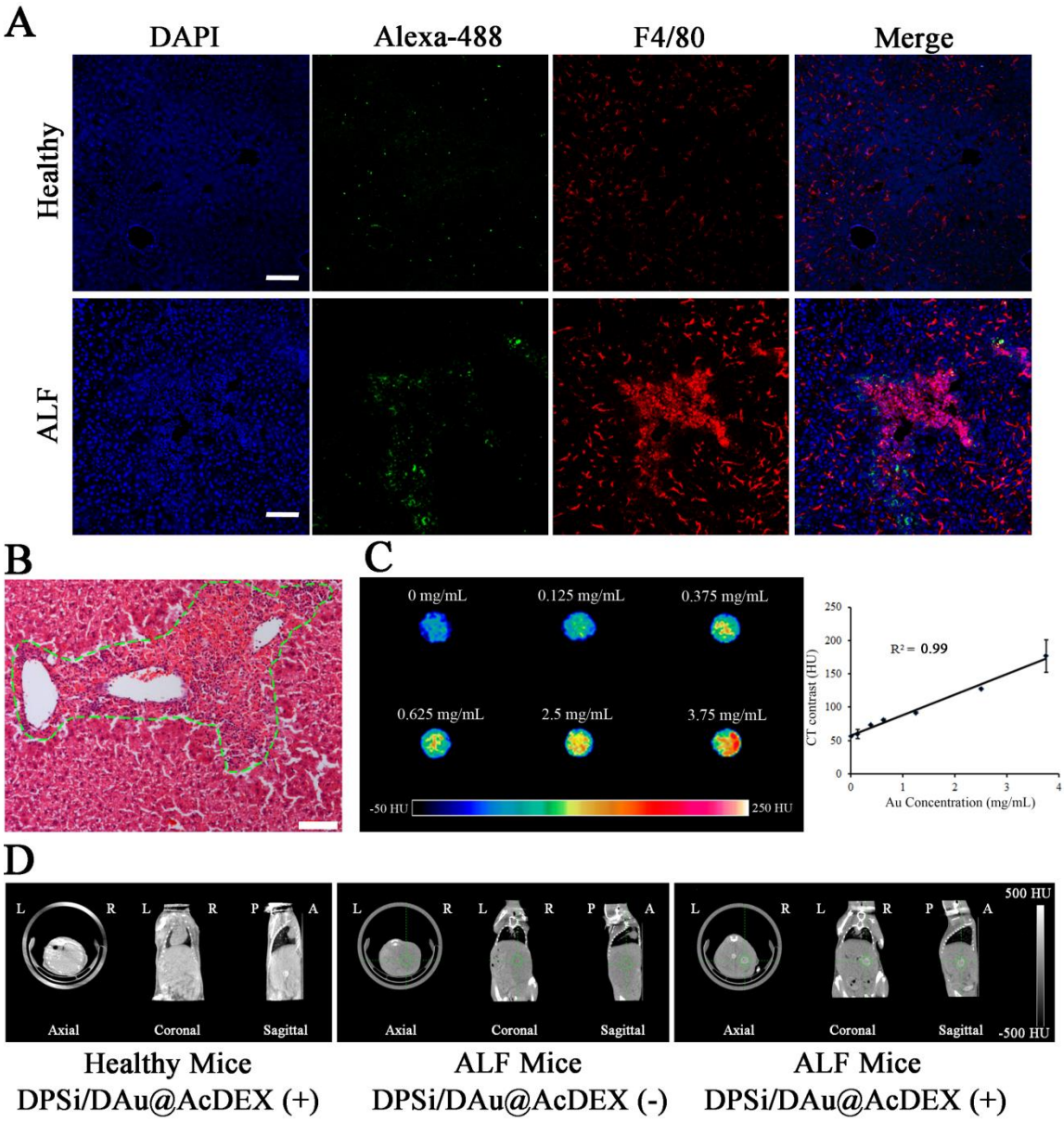

Figure 4. (A) Immunofluorescence images of healthy liver or ALF liver after *i.v.* administrated with Alexa-488 labeled DPSi/DAu@AcDEX. All scale bars indicate 100 μm. **(B)** H&E staining of ALF liver, suggesting the lesion specific macrophages accumulation. All scale bars indicate 100 μm. **(C)** CT-images of the DPSi/DAu@AcDEX aqueous dispersion with different concentrations and CT value (HU) of DPSi/DAu@AcDEX at different concentration of DAu. **(D)** *In vivo* axial, coronal and sagittal CT images of ALF mice in absence of *i.v.* administration of DPSi/DAu@AcDEX, healthy mice after *i.v.* administration of DPSi/DAu@AcDEX, and ALF mice after *i.v.* administration of DPSi/DAu@AcDEX.

Healthy or ALF C57BL/6 mice after *i.v.* injected with 200 μL of DPSi/DAu@AcDEX at 20 mg kg^{-1} of DAu.

In summary, we have successfully prepared a PSi-based nanohybrid composite for liver regeneration and ALF treatment. This system can be used to identify pathologically changes in the tissues and selectively deliver drugs to these sites, which have an extremely high potential to ameliorate therapeutic outcomes for patients. It also effectively loads the therapeutic compound (XMU-MP-1) inside, which greatly improves the drug solubility, precise *in situ* drug delivery and the drug functioning time. *In vivo* results confirmed the superior treatment effect and better compliance of this newly developed nanoformulation than free compound. Considering our data, the application of our nanosystem appears to play a crucial role in targeting the lesion area, thus an increased local drug concentration may attribute to the improved ALF reverse effect. Moreover, the residence of Au particles within the matrix further endows our system for CT-imaging, which shows promise to diagnose ALF at an early stage. Altogether, these results support that the developed nanohybrid has a potential theranostic platform for ALF.

Acknowledgements

Dr. W. Li acknowledges the Orion Research Foundation for financial support. Dr. D.F. Liu and Prof. H. Zhang acknowledge Jane and Aatos Erkko Foundation (Decision No. 4704010) for financial support. Prof. H. Zhang acknowledges financial support from Academy of Finland (Grant No. 297580). Prof. X. Deng acknowledges financial support from the Ministry of Science and Technology (Grants No. 2016YFA0502001 and 2017YFA0504500) and the National Natural Science Foundation of China (grants No. 81422045, U1405223 and 81661138005), the Fundamental Research Funds for the Central Universities of China (grant

No. 20720160064), and the Program of Introducing Talents of Discipline to Universities (111 Project, B12001). Prof. D. Zhou acknowledges financial support from the National Natural Science Foundation of China (Grant No. 31625010) and the Ministry of Science and Technology (Grant No. 2017YFA0504500). Prof. H.A. Santos acknowledges financial support from the University of Helsinki Funds, the Sigrid Juselius Foundation (Decision no. 4704580), and the European Research Council under the European Union's Seventh Framework Programme (FP/2007-2013, Grant No. 310892).

Received: ((will be filled in by the editorial staff))

Revised: ((will be filled in by the editorial staff))

Published online: ((will be filled in by the editorial staff))

[1] H. He, N. Zheng, Z. Song, K. H. Kim, C. Yao, R. Zhang, C. Zhang, Y. Huang, F. M. Uckun, J. Cheng, L. Yin, *ACS Nano* **2016**, *10*, 1859.

[2] H. Wang, C. A. Thorling, X. Liang, K. R. Bridle, J. E. Grice, Y. Zhu, D. H. Crawford, Z. P. Xu, X. Liu, M. S. Roberts, *J. Mater. Chem. B* **2015**, *3*, 939.

[3] Z. Guo, M. Gao, M. Song, Y. Li, D. Zhang, D. Xu, L. You, L. Wang, R. Zhuang, X. Su, *Adv. Mater.* **2016**, *28*, 5898.

[4] C. Zhang, X. Qu, J. Li, H. Hong, J. Li, J. Ren, G. F. Payne, C. Liu, *Adv. Healthcare Mater.* **2015**, *4*, 1972.

[5] A. Lamprecht, *Nat. Rev. Gastroenterol. Hepatol.* **2015**, *12*, 195.

[6] R. Bansal, B. Nagórniewicz, G. Storm, J. Prakash, *J. Hepatol.* **2017**, *66*, S43.

[7] S. Kirschner, B. Mürle, M. Felix, A. Arns, C. Groden, F. Wenz, A. Hug, G. Glatting, M. Kramer, F. A. Giordano, M. A. Brockmann, *PloS One* **2016**, *11*, e0165994.

[8] M. D. Torres, R. D. Stevens, A. Gurakar, *Gastroenterol. Hepatol.* **2010**, *6*, 444.

[9] F. Fan, Z. He, L. L. Kong, Q. Chen, Q. Yuan, S. Zhang, J. Ye, H. Liu, X. Sun, J. Geng, L. Yuan, L. X. Hong, X. C., Z. W. J., X. H. Sun, Y. Z. Li, P. Wang, L. H. Huang, X. R. Wu, Z. L. Ji, Q. Wu, N. S. Xia, N. S. Gray, L. F. Chen, C. H. Yun, X. M. Deng, D. W. Zhou, *Sci. Transl. Med.* **2016**, *8*, 352.

[10] Z. Liu, V. Balasubramanian, C. Bhat, M. Vahermo, E. Mäkilä, M. Kemell, F. Fontana, A. Janoniene, V. Petrikaite, J. Salonen, H. A. Santos, *Adv. Healthcare Mater.* **2017**, *6*, 1601009.

[11] A. Janoniene, Z. Liu, L. Baranauskiene, E. Mäkilä, M. Ma, J. Salonen, J. Hirvonen, H. Zhang, V. Petrikaite, H. A. Santos, *ACS Appl. Mater. Interfaces* **2017**, *9*, 13976.

[12] N. Shrestha, F. Araújo, M. A. Shahbazi, E. Mäkilä, M. J. Gomes, B. Herranz‐Blanco, R. Lindgren, S. Granroth, E. Kukk, J. Salonen, H. A. Santos, *Adv. Funct. Mater.* **2016**, *26*, 3405.

[13] M. P. Ferreira, S. Ranjan, A. M. Correia, E. M. Mäkilä, S. M. Kinnunen, H. Zhang, M.-A. Shahbazi, P. V. Almeida, J. J. Salonen, H. J. Ruskoaho, H. A. Santos, *Biomaterials* **2016**, *94*, 93.

[14] F. Fontana, M. A. Shahbazi, D. Liu, H. Zhang, E. Mäkilä, J. Salonen, J. T. Hirvonen, H. A. Santos, *Adv. Mater.* **2016**.

[15] M.-A. Shahbazi, T. D. Fernández, E. M. Mäkilä, X. Le Guével, C. Mayorga, M. H. Kaasalainen, J. J. Salonen, J. T. Hirvonen, H. A. Santos, *Biomaterials* **2014**, *35*, 9224.

[16] J. A. Santoslópez, A. Garcimartín, P. Merino, M. E. Lópezoliva, S. Bastida, J. Benedí, F. J. Sánchezmuniz, *PLoS One* **2016**, *11*, 147469.

[17] G. Kwak, *Oxid. Med. Cell. Longevity* **2016**, *2016*, 3928714.

[18] K. R. Beavers, T. A. Werfel, T. Shen, T. E. Kavanaugh, K. V. Kilchrist, J. W. Mares, J. S. Fain, C. B. Wiese, K. C. Vickers, S. M. Weiss, *Adv. Mater.* **2016**, *28*, 7984.

[19] A. O. Shakil, B. C. Jones, R. G. Lee, M. P. Federle, J. J. Fung, J. Rakela, *Dig. Dis. Sci.* **2000**, *45*, 334.

[20] L. A. Austin, B. Kang, M. A. El-Sayed, *Nano Today* **2015**, *10*, 542.

[21] Y. Dou, Y. Guo, X. Li, X. Li, S. Wang, L. Wang, G. Lv, X. Zhang, H. Wang, X. Gong, C. Jing, *ACS Nano* **2016**, *10*, 2536.

[22] S. B. Lee, H. W. Lee, T. D. Singh, Y. Li, S. K. Kim, S. J. Cho, S.-W. Lee, S. Y. Jeong, B.-C. Ahn, S. Choi, *Theranostics* **2017**, *7*, 926.

[23] P. Chhour, P. C. Naha, S. M. O'Neill, H. I. Litt, M. P. Reilly, V. A. Ferrari, D. P. Cormode, *Biomaterials* **2016**, *87*, 93.

[24] P. Chhour, J. Kim, B. Benardo, A. Tovar, S. Mian, H. I. Litt, V. A. Ferrari, D. P. Cormode, *Bioconjugate Chem.* **2016**, *28*, 260.

[25] S. Wang, P. Huang, X. Chen, *Adv. Mater.* **2016**, *28*, 7340.

[26] L. Qiu, T. Chen, I. Öçsoy, E. Yasun, C. Wu, G. Zhu, M. You, D. Han, J. Jiang, R. Yu, W. Tan, *Nano Lett.* **2014**, *15*, 457.

[27] D. Liu, H. Zhang, E. Mäkilä, J. Fan, B. Herranzblanco, C. F. Wang, R. Rosa, A. J. Ribeiro, J. Salonen, J. Hirvonen, H. A. Santos, *Biomaterials* **2015**, *39*, 249.

[28] P. M. Valencia, P. A. Basto, L. Zhang, M. Rhee, R. Langer, O. C. Farokhzad, R. Karnik, *ACS Nano* **2010**, *4*, 1671.

[29] E. M. Bachelder, E. N. Pino, K. M. Ainslie, *Chem. Rev.* **2016**, *117*, 1915.

[30] J. L. Cohen, S. Schubert, P. R. Wich, L. Cui, J. A. Cohen, J. L. Mynar, J. M. Fréchet, *Bioconjugate Chem.* **2011**, *22*, 1056.

[31] E. M. Bachelder, T. T. Beaudette, K. E. Broaders, J. Dashe, J. M. Fréchet, *J. Am. Chem. Soc.* **2008**, *130*, 10494.

[32] J. Riikonen, A. Correia, M. Kovalainen, S. Näkki, M. Lehtonen, J. Leppänen, J. Rantanen, W. Xu, F. Araújo, J. Hirvonen, H. A. Santos, V. P. Lehto, *Biomaterials* **2015**, *52*, 44.

[33] Y. N. Zhang, W. Poon, A. J. Tavares, I. D. Mcgilvray, W. C. Chan, *J. Controlled Release* **2016**, *240*, 332.

[34] K. Ray, *Nat. Rev. Gastroenterol. Hepatol.* **2016**, *13*, 560.

[35] K. M. Tsoi, S. A. Macparland, X. Z. Ma, V. N. Spetzler, J. Echeverri, B. Ouyang, S. M. Fadel, E. A. Sykes, N. Goldaracena, J. M. Kaths, J. B. Conneely, B. A. Alman, M. Selzner, M. A. Ostrowski, O. A. Adeyi, A. Zilman, I. D. Mcgilvray, W. C. W. Chan, *Nat. Mater.* **2016**, *15*, 1212.

[36] B. Wang, X. He, Z. Zhang, Y. Zhao, W. Feng, *Acc. Chem. Res.* **2013**, *46*, 761.

[37] D. Zhou, C. Conrad, F. Xia, J. S. Park, B. Payer, Y. Yin, G. Y. Lauwers, W. Thasler, J. T. Lee, J. Avruch, N. Bardeesy, *Cancer Cell* **2009**, *16*, 425.

[38] S. Zhang, Q. Chen, Q. Liu, Y. Li, X. Sun, L. Hong, S. Ji, C. Liu, J. Geng, W. Zhang, Z. Lu, Z. Yin, Y. Zeng, K.-H. Lin, W. Qiao, Q. Li, K. Nakayama, K. Nakayama, X. Deng, R. Johnson, L. Zhu, D. Gao, L. Chen, D. Zhou, *Cancer Cell* **2017**, *31*, 669.

[39] K. A. Rose, N. S. Holman, A. M. Green, M. E. Andersen, E. L. Lecluyse, *J. Pharm. Sci.* **2016**, *105*, 950.

[40] A. M. Larson, J. Polson, R. J. Fontana, T. J. Davern, E. Lalani, L. S. Hynan, J. S. Reisch, F. V. Schiødt, G. Ostapowicz, A. O. Shakil, *Hepatology* **2006**, *43*, 1364.

[41] A. Pellicoro, P. Ramachandran, J. P. Iredale, J. A. Fallowfield, *Nat. Rev. Immunol.* **2014**, *14*, 181.

[42] T. A. Wynn, A. Chawla, J. W. Pollard, *Nat.* **2013**, *496*, 445.

[43] S. Yasui, K. Fujiwara, K. Okitsu, Y. Yonemitsu, H. Ito, O. Yokosuka, *Hepatol. Res.* **2012**, *42*, 42.

[44] M. Romero, S. L. Palmer, J. A. Kahn, L. Ihde, L. M. Lin, A. Kosco, R. Shinar, A. Ghandforoush, L. S. Chan, L. M. Petrovic, L. Sher, T.-L. Fong, *Dig. Dis. Sci.* **2014**, *59*, 1987.

[45] E. Ozaslan, C. Efe, N. G. Ozaslan, *Dig. Dis. Sci.* **2015**, *60*, 2847.

Figure 1

Click here to access/download

Production Data

Figure 1.tif

Figure 2

Figure 3

Click here to access/download

Production Data

Figure 3.tif

Figure 4

Graphical Abstract